The Journal of the Astronautical Sciences, Vol. 58, No. 2, April–June 2011, pp. 275–290

A Study of the Achievable Geosynchronous Angles-Only Orbit Estimation Accuracy

Jill Tombasco[1] and Penina Axelrad[2]

Abstract

This analysis investigates the geosynchronous orbit estimation accuracy that can be achieved given short-term dedicated tracking by a single ground-based optical sensor. Two Global Positioning System (GPS) Wide Area Augmentation System (WAAS) satellites are chosen for this case study because highly-accurate WAAS reference position and velocity point solutions are available for public use and present the opportunity to experimentally assess the effect of orbit perturbations to the meter level. Simulated optical (angles-only) observations are generated from these experimental reference ephemerides. By varying the tracking parameters of nightly tracking arc length, sampling rate, and orbit epoch, and fitting to two consecutive days of observations, a batch estimation analysis is performed that characterizes the expected level of two-day solution accuracy given an imperfect dynamic model and a satellite which is performing small, frequent maneuvers. The results show that the estimated solution fits over the two-day period to better than 10 meters. An analysis of one month of data for an uncontrolled satellite is performed to statistically determine the solution uncertainty and mean accuracy. It is shown that 10-meter accuracy is possible given short sampling intervals (10 to 30 seconds) and long nightly track lengths (three or more hours per night). Several tracking scenarios are found to meet accuracy requirements on the order of 10 to 100 meters.

Introduction

According to the European Space Agency (ESA) Database and Information System Characterizing Objects in Space (DISCOS), approximately 1,040 cataloged objects pass through the geosynchronous orbit. Of these, only about 30% are active objects [1]. Because of the importance of the geosynchronous orbit for communication purposes, the large number of uncontrollable or otherwise uncooperative objects, and the fact that objects are not removed via natural perturbations, it is essential to fully characterize the orbit estimation accuracy possible via passive tracking techniques. Accurate knowledge of the current and predicted locations and the associated uncertainty of both uncontrolled and controlled objects enhances

[1]Graduate Student, Aerospace Engineering Sciences Department, University of Colorado, Boulder, CO.
[2]Professor, Aerospace Engineering Sciences Department, University of Colorado, Boulder, CO.

observation association, collision prediction and avoidance, and detection of spacecraft maneuvers.

The estimation of geosynchronous orbits using ground-based angles-only measurements is a challenge because of the very slight geometrical variation of the observations, uncertainties in the dynamic model, and the temporal and weather limitations to ground-based optical tracking. Fortunately, in many cases an orbit solution is required after only a day or two of optical tracking and is not required in real time. It is therefore of interest to characterize the short-term tracking requirements necessary to obtain a specified geosynchronous orbit accuracy using optical tracking from a single ground station; conversely, it is desirable to understand the orbit accuracy possible given limited tracking coverage and observation sampling rates. This knowledge is essential for track planning and resource allocation. This work investigates the impact of nightly track length, sampling interval, orbit epoch location, and realistically mismodeled spacecraft dynamics on estimation accuracy.

Angles-only geosynchronous orbit estimation with data arcs on the order of one week have been well characterized by Sabol and Culp [2, 3]. Simulation studies showed that because of the difficulty in estimating the radial position using optical data, 10-meter accuracy estimates are possible with one week of tracking. In particular, the semimajor axis cannot be accurately estimated given only one night of tracking as the offset from the nominal geosynchronous semimajor axis is manifested only in the slowly drifting azimuth measurement. Ranging data allow for a more accurate and quicker estimate of the orbit states, including the semimajor axis. The addition of range measurements to the angular data results in five-meter orbit accuracy [3]. Follow-on research presented in references [4, 5] utilizes optical observations of TDRS-5 (Tracking and Data Relay Satellite) collected with a high-accuracy optical sensor. Comparisons to TDRS reference osculating element sets, which are accurate to tens of meters and available from the NASA Flight Dynamics Facility (FDF), [6]. The position errors are shown to be approximately five meters in the radial direction and 10 meters in both cross-track and along-track components.

Recent research by Vallado and his colleagues on geosynchronous debris has focused on the orbit estimation accuracy achievable utilizing angles-only optical observations and the fusion of international data sources for collision avoidance [7, 8]. Their work uses optical observations collected by the International Scientific Observing Network (ISON), a cooperative network of global sensors capable of providing ground-based coverage of the entire geosynchronous belt [9]. Experimental optical observations of several individual objects are processed with an initial orbit determination, the results of which are fed into a least-squares batch processor followed by a filter-smoother. It was shown that 10 to 15 observations per day over the course of three to four days produced orbit accuracy on the order of a few kilometers.

Research on sparse angles-only geosynchronous orbit estimation has also been conducted by the Kashima Space Communications Center, Communications Research Laboratory, Japan [10]. Kawase theoretically computes optical orbit determination error for geosynchronous satellites using one to two consecutive nights of line-of-sight measurements collected only once or twice per evening. Utilizing first order linearized equations of unperturbed satellite motion, theoretical expressions are developed which express orbit element estimation uncertainty as a function of the angular separation between observations. Given one day of data collected over

a six hour period and measurement noise on the order of one arcsecond, Kawase finds the expected orbit uncertainty to be on the order of one kilometer.

In contrast, this work empirically determines the relationship between tracking parameters and estimation accuracy using variational equations to model realistically perturbed geosynchronous dynamics. High-precision reference ephemerides of the Wide Area Augmentation System (WAAS) satellites provide a unique opportunity to empirically investigate orbit estimation techniques with publicly available experimental data that is accurate to the meter level. This is a significant accuracy improvement over the commonly-used TDRS reference osculating elements, which are provided for a single epoch and are accurate to approximately 30 to 40 meters [6]. The nonlinear variational equations utilized in this study have been developed for a set of hybrid elements [11]. The achievable accuracy of angles-only orbit estimation is determined by fitting to two consecutive days of optical measurements while varying the tracking parameters of nightly track length, observation sampling interval, and orbit epoch location. Two consecutive days of data are processed in order to accurately recover the semimajor axis. To assess the short-term orbit determination accuracy it is necessary to compare the estimated orbit solution and uncertainty against a reference orbit. Although simulation studies can provide a perfectly-known reference orbit and observations of the object, simulated observations do not capture the complexities of actual measurements and geosynchronous orbital dynamics. Conversely, experimental measurements reflect realistic dynamics but can be degraded with unknown time-varying and constant biases, which in turn introduce unexpected error into the orbit solution. To overcome the respective drawbacks of simulated and experimental observations, this work builds a simulation study around the daily point solutions of WAAS satellites.

WAAS is an augmentation to GPS provided by the Federal Aviation Administration (FAA) to improve the integrity and accuracy of GPS for aviation use. WAAS nominally comprises a network of ground-based Wide-Area Master Stations and Reference Stations spanning North America, and two geosynchronous satellites that transmit pseudorandom ranging signals and position, clock and atmospheric corrections to North American user receivers [12]. The Reference Stations track the WAAS satellites pseudorange signals, and from this tracking data the WAAS reference position and velocity point solutions are estimated [13]. The reference ephemerides are produced using a high-precision GPS solution code, which was based on the Real Time Gipsy code from the Jet Propulsion Laboratory [14]. The uncertainty in these solutions is reported to be at the level of 10 meters per axis. WAAS users who incorporate the additional ranging measurement from the geostationary satellite, rely on these orbit predictions in their position solutions. Many users only depend on the WAAS for corrections and integrity for the GPS satellites, and are completely unaffected by the accuracy of the WAAS orbits.

The Earth-Centered Earth-Fixed (ECEF) position and velocity point-solutions of each WAAS satellite are provided 24 hours per day at 256-second intervals [15]. An archive of the reference point-solutions is publicly accessible through the FAA [16]. Though sensitive to measurement noise, the reference ephemerides are reported to be accurate to better than 10 meters, even over spacecraft maneuvers [13].

As of November 2010, three WAAS satellites are on orbit: Anik F1R, Inmarsat 4F3, and Galaxy 15. Galaxy 15 failed on orbit on April 5, 2010, and has

TABLE 1. Variation Parameters for Batch Estimation Analysis

Nightly Track Length	Sampling Interval
10 min	10 sec
30 min	30 sec
1 hr	256 sec
3 hr	1800 sec
6 hr	3600 sec

subsequently been operationally replaced for WAAS transmissions by Inmarsat 4F3 [17]. It is believed that the spacecraft failure was caused by intense solar activity [17]. It has resulted in the satellite being unresponsive to ground commands, but still capable of broadcasting WAAS signals. After the failure Galaxy 15 drifted within close proximity of several active geosynchronous satellites and continued to drift through the geosynchronous belt until December 23, 2010 [18, 19, 20]. At that time, the onboard battery completely drained and the satellite reset itself, allowing Galaxy 15 to begin accepting control commands once again [20]. During the time it was inactive, Galaxy 15 was a unique uncontrolled satellite in that it was not maneuvering, but it continued to actively broadcast its GPS-like pseudorange signal. Additionally, the WAAS ground segment continued to observe these signals and estimate the satellite's orbit. The WAAS reference ephemerides provided between April 5 and December 23 can therefore be used to assess the estimation accuracy of controlled and uncontrolled WAAS satellites.

Approach

This empirical analysis takes advantage of the high-accuracy WAAS reference ephemerides. First, simulated optical observations are generated from a two-day span of the reference ephemeris. Subsets of the simulated continuous observations are then created for a given set of nightly track length, sampling interval, and observation epoch time. A hybrid element batch estimator [11] is utilized to process each observation subset individually, and the estimated solution is differenced from the reference ephemeris. The three-dimensional (3D) ECEF position errors over the two-day fit period, quantified by the Root Mean Square (RMS), are compared for all subset solutions.

Track Length and Sampling Interval Variation

Simulated continuous azimuth and elevation measurements of Anik F1R and Galaxy 15 are generated from the reference ECEF ephemerides of May 2010. The reference observations, generated at the reference sampling interval of 256 seconds, are interpolated at the selected sampling rate for the chosen nightly track length. Gaussian noise of mean of zero arcseconds and standard deviation of one arcsecond is added to the observations to replicate the measurement noise expected in experimental observations [3].

The tracking parameters varied for this study are shown in Table 1. The shorter sampling intervals (10–30 seconds) are practical assuming dedicated tracking of a single object, whereas the longer sampling intervals (1,800–10,800 seconds) are applicable in a tracking scenario where more than one object must be tracked

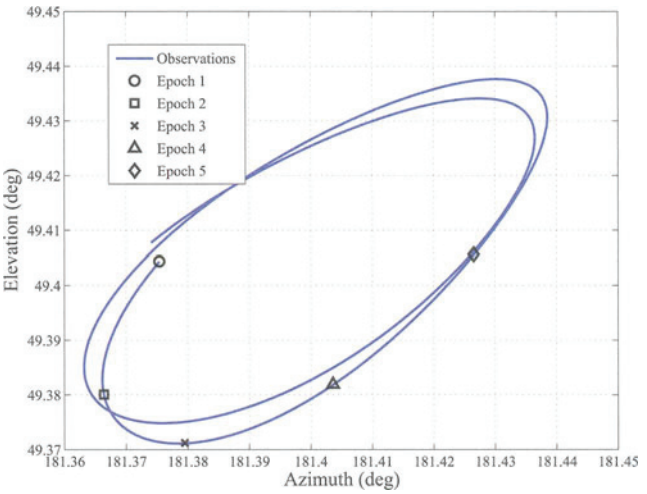

FIG. 1. Anik F1R Reference Observations and Selected Epoch Locations (May 2 to May 3, 2010).

through the night and the sensor is able to revisit the objects. Track lengths of 30 minutes to six hours per night are reasonable for optical tracking which depends on the proper lighting conditions and clear skies. Cases in which fewer than three observation pairs are available are not processed as the number of estimated parameters would be greater than the number of observations.

Observed Orbit Geometry Variation

A geosynchronous object traces out an elliptical pattern that drifts slowly in azimuth relative to an Earth-fixed vantage point. An example of this motion is depicted in Fig. 1, which shows the azimuth and elevation measurements of Anik F1R on May 2 and 3, 2010 as seen by an observer in Albuquerque, New Mexico. It takes approximately 24 hours for the satellite to traverse one ellipse. The motion is largely repeatable and the entire azimuth and elevation span is less than 0.2 degrees. For comparison, Fig. 2 displays the azimuth and elevation measurements of Galaxy 15 as seen from the same ground station. The observations are plotted for May 1 through May 5, 2010, approximately one month after the spacecraft's failure. Unlike Anik F1R, the drift rate of Galaxy 15 is significantly faster than that of the Earth and it shifts in both azimuth and elevation. This behavior is typical of an inactive geosynchronous satellite that is not controlled to remain near its nominal mean longitude and radial distance. Reference measurements corresponding to five epochs for Anik F1R are marked in the figure. The epochs are listed in Table 2.

The geosynchronous orbit location, shape, and drift are dictated by the satellite's orbital elements; the semimajor axis offset from the nominal geosynchronous semimajor axis is directly proportional to the azimuthal drift, the inclination sets the tilt angle relative to the azimuth plane, and the eccentricity determines the ellipse proportions. The mean azimuth is set by the mean longitude and the ellipse pinching, or nodal crossing point, is a function of right ascension of the ascending node and semimajor axis [21]. The observation geometry may affect the accuracy of the estimated orbit as the ellipse characteristics are tied to different orbit elements. For example, the semimajor axis can only be recovered accurately by

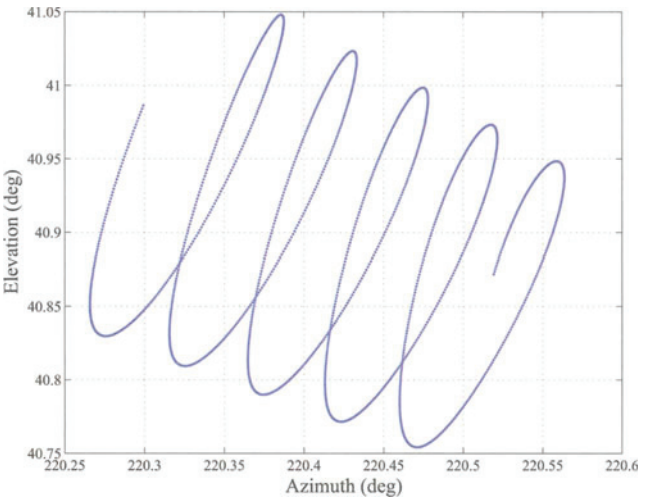

FIG. 2. Galaxy 15 Reference Observations (May 1 to May 5, 2010).

observing the time-variation of the azimuth measurements. To see this effect we will shift the observation epoch to vary the orbit section that is observed and compare the respective estimated solutions. The observations shown in Fig. 1 begin at Epoch 1, which corresponds to a UTC time of 00:01:04 on May 2. Results will be shown for a range of observation epochs shifted by three-hour increments. This ensures that track lengths beginning at each of the five selected epochs provide unique geometries, including the nodal crossing point. This epoch shifting covers only one-half of the orbit ellipse because of the near-symmetry about the minor and major ellipse axes.

Hybrid Element Batch Estimation

The batch estimation is performed in terms of the hybrid elements, which are defined as

$$\mathbf{X}^{\mathrm{T}} = [\ \lambda \quad \Delta\bar{a} \quad P_1 \quad P_2 \quad Q_1 \quad Q_2\ ]$$

The hybrid element set comprises the Earth-fixed sub-satellite longitude (λ), the longitudinal drift rate ($\Delta\bar{a}$), eccentricity vector components (P_1, P_2), and the inclination vector components (Q_1, Q_2). These elements have been shown to be well-defined for near-geosynchronous orbits and their variations are numerically stable for propagation of geosynchronous perturbed motion. The elements exhibit

TABLE 2. Shifted Observation Epochs for Anik F1R

Epoch Number	UTC on May 2, 2010
1	00:01:04
2	03:01:04
3	06:01:04
4	09:01:04
5	12:01:04

TABLE 3. Physical Parameters of Anik F1R and Galaxy 15

Satellite	Area (m^2)	Mass (kg)	Reflectivity Coefficient	Effective Area-to-Mass Ratio (m^2/kg)
Anik F1R	121.25	3015	0.985	0.040
Galaxy 15	76.08	1892	0.547	0.022

small, near-linear variations for perturbed motion, and as such batch estimation is an appropriate orbit determination strategy. It follows that the covariance matrix can be accurately propagated via the state transition matrix. Furthermore, the azimuth measurement sensitivity to the hybrid elements does not suffer from loss of second-order influences, which has been shown to adversely impact geosynchronous orbit estimation in the inertial Cartesian state space [11].

The batch estimator is initialized for each case by interpolating the reference ephemerides to the observation epoch time. The *a priori* covariance is set to an uncertainty level of one kilometer in each ECI position component and one centimeter per second in each velocity component. To map the *a priori* covariance into the hybrid element state space, 1000 randomly-sampled ECI state vectors, deviated from the truth vector according to the defined *a priori* values, are transformed into hybrid element state vectors. The distribution of the error from the expected hybrid element state vector represents the *a prio*ri nondiagonal covariance matrix. The equations of motion are numerically integrated to propagate the satellite's orbit over the two day observation period. The dynamic model includes perturbations because of the Earth gravity field, lunisolar point mass gravity, and solar radiation pressure acting on a spherical satellite of constant reflectivity with the Earth shadow modeled cylindrically. The effective area-to-mass ratios of Anik F1R and Galaxy 15 are determined empirically.

Determination of Effective Area-to-Mass Ratio

The reported surface area and launch mass of Anik F1R and Galaxy 15 are shown in Table 3 [22, 23]. Galaxy 15's surface area is not provided by reference [23] and is assumed to be scaled by the mass ratio of Galaxy 15 to Anik F1R, a viable assumption for geosynchronous communication satellites.

A priori knowledge of the spacecraft physical parameters that affect the solar pressure perturbation leads to a more accurate dynamic model. The reflectivity values of high-gain antennas and solar panels, which make up the bulk of the communication spacecraft surface area, have been experimentally found to be approximately 1.2 to 1.3 [24]. As the reflectivity coefficients of Anik F1R and Galaxy 15 are not perfectly known, batch estimation is used to determine an appropriate solar reflectivity coefficient for each satellite. It is expected that the reflectivity coefficients of Anik F1R and Galaxy 15 will be near the range of typical communication satellites. The Anik F1R ECEF position vector components over two days in January 2010 are processed as observations by a batch estimator to solve for the reflectivity coefficient. Given the physical parameters shown in Table 3, a simple cannonball with a cylindrical Earth shadow is used to model the solar pressure orbit perturbation. Additionally, a 4×4 Earth gravitational field and lunisolar third body point mass gravitational forces are included in the dynamic model. An 8×8 gravity field is known to be sufficient for most geosynchronous

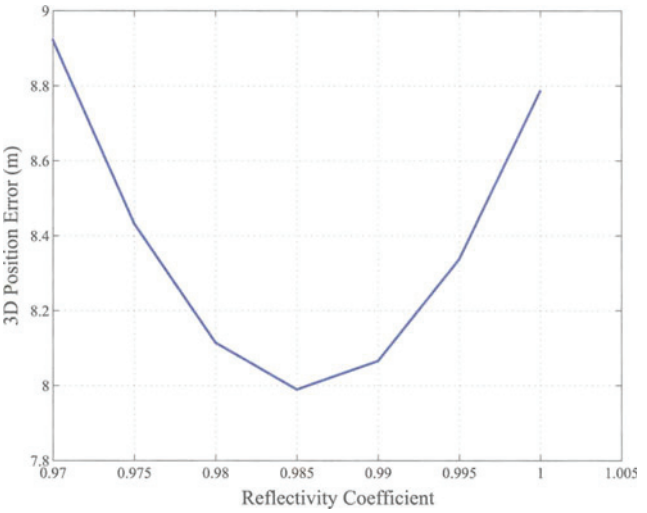

FIG. 3. Effect of Reflectivity Coefficient on Anik F1R 3D ECEF Position Error RMS.

orbit estimation applications [25]. The inclusion of an 8×8 gravity field was investigated, and it was determined that a gravity field of order and degree larger than four is unnecessary because of the dynamic model accuracy limitations introduced by the solar pressure error. The 3D ECEF position error RMS value is computed and stored; the batch estimator is then re-initialized and repeated with a new reflectivity coefficient. In this manner, the batch processor sweeps through reflectivity coefficients between 0 and 2 at intervals of 0.1.

Figures 3 and 4 present the 3D ECEF position and velocity error RMS of Anik F1R as a function of reflectivity coefficient for a more refined search grid. A reflectivity coefficient of 0.985 produces the minimum position error RMS value of eight meters and the minimum velocity error of 3.325 millimeters per seconds. This reflectivity value is now assigned as Anik F1R's reflectivity coefficient throughout the remainder of the analysis. Likewise, using two days of data from

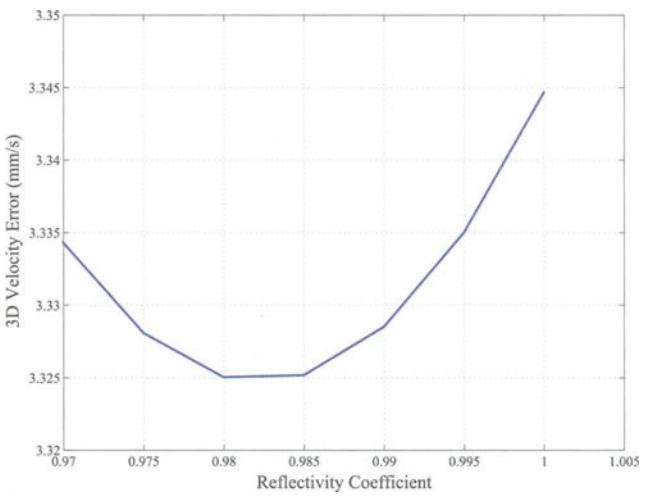

FIG. 4. Effect of Reflectivity Coefficient on Anik F1R 3D ECEF Velocity Error RMS.

May 2010, Galaxy 15's reflectivity coefficient is determined to be 0.547. Note that the reflectivity coefficient of Galaxy 15 determined with pre-failure data is approximately 0.65, indicating that Galaxy 15's solar panels may have been pointed off-nominal prior to the failure. Numerous two-day fits were performed for both Anik F1R and Galaxy 15, and the reflectivity coefficient profiles do not significantly depend on which two-day data sets are processed. The effective reflectivity coefficients for the simplified solar radiation pressure model are lower than the more nominal values of 1.2 to 1.3 because of the satellite's solar arrays not pointing directly at the Sun.

Anik F1R and Galaxy 15 Analyses

Initially, observations of Anik F1R spanning May 2 and 3, 2010 are processed. The ECEF 3D RMS position error values for each estimate are inspected to determine the achievable estimation accuracy for a given sampling interval and track length. The impact of epoch location is analyzed by comparing the 3D position error RMS values for each epoch given a selected track length.

To best evaluate the batch performance, position solutions from the batch estimator are compared to the reference ephemerides. Although the batch processor does provide a formal covariance that can be propagated to any time within the data set, the formal estimated statistics do not capture the dynamic model uncertainty. Therefore the error distribution will be empirically determined using a large set of results for each sampling interval and track length combination. The mean error and error uncertainty are experimentally determined by processing sliding two-day data windows over the course of one month and examining the average and deviation of the estimation accuracy for each tracking parameter combination. Controlled geosynchronous satellites typically perform large station keeping maneuvers every one to three weeks [21]. To avoid estimation issues because of fitting over large maneuvers, the uncertainty analysis is performed by fitting to the reference observations of Galaxy 15 from May 2 to May 30, 2010. The tracking parameters of coverage arc length and sampling rate are varied as shown in Table 1. Because of the significant drift rate of Galaxy 15 relative to the Earth, any epoch-dependent estimation effects will be averaged out over one month and the observation epoch variation is not included in the Galaxy 15 analysis.

Analysis of Satellite Dynamics

The Anik F1R continuous two-day reference ephemeris is processed by the batch estimator in order to assess how well the dynamic model captures realistic satellite dynamics. The position and velocity component errors throughout the fit period are shown in Figs. 5 and 6. The solution error is on the order of 10 meters in all three position components, and less than one centimeter per second in velocity. The 3D position error RMS is 6.7 meters. The systematic difference between the estimated solution and reference point solution is because of unmodeled dynamics; in particular, the cannonball solar pressure model is not ideal for the geometry of a geosynchronous communication satellite, in which the surface area is typically dominated by large solar panels. The fit error lies predominantly in the Z component most likely because of the cannonball solar pressure model not incorporating out-of-plane effects.

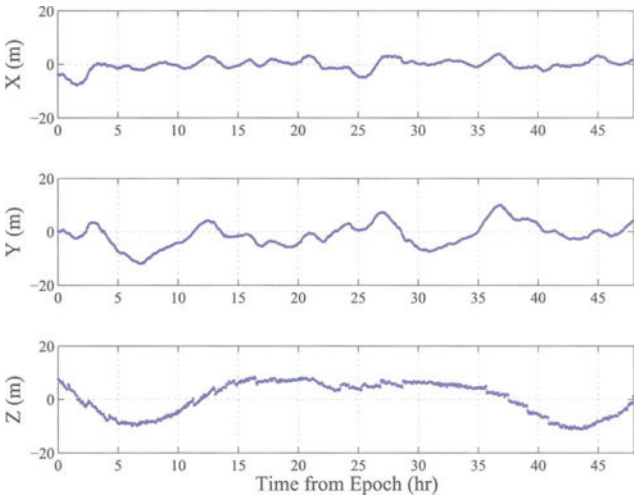

FIG. 5. ECEF Position Error for Two-Day Anik F1R Batch Estimation.

It can be seen that the Z direction velocity error is dominated by discontinuities on the order of one centimeter per second. The Z position error also displays meter-level discontinuities. Because the batch solution is continuous by definition, the discontinuities must exist in the reference point solutions. Given the periodic nature of the discontinuities, it was hypothesized that they are introduced via either the estimation process used to form the WAAS reference ephemerides or by actual spacecraft maneuvers.

Inspection of the Galaxy 15 two-day batch fit error before and after the April 5, 2010 on-orbit failure allows a unique opportunity to experimentally determine the discontinuity source by contrasting fit errors for a controlled object to an identical uncontrolled object. Tenth-order polynomials are fit to Galaxy 15 one-day reference orbits before and after the spacecraft failure. Applying a general polynomial fit rather than batch estimating the fit ensures that no errors are introduced by

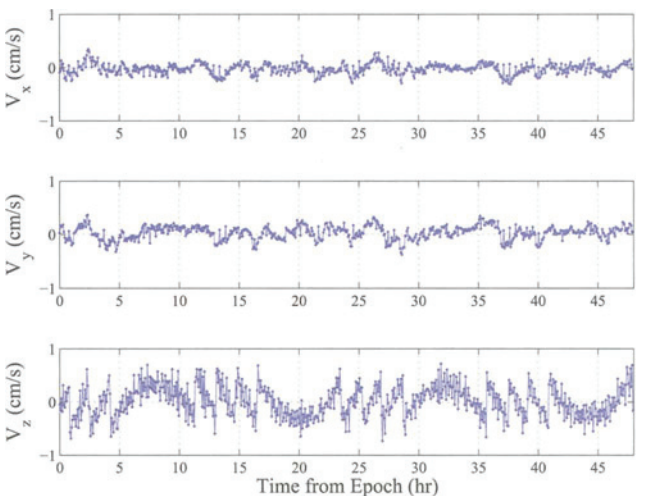

FIG. 6. ECEF Velocity Error for Two-Day Anik F1R Batch Estimation.

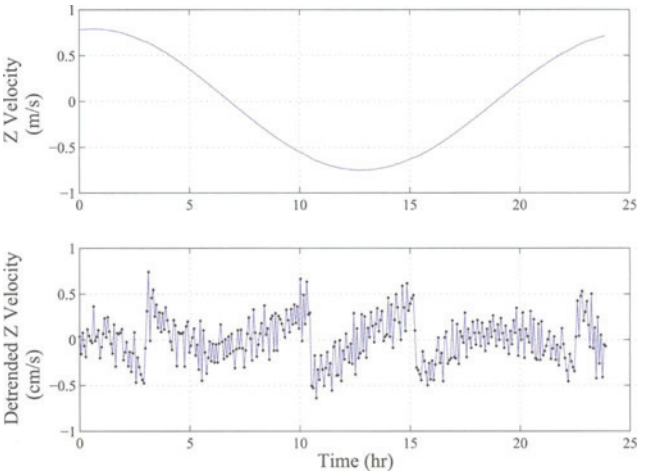

FIG. 7. Galaxy 15 Z Velocity and Fit Error (January 19, 2010).

inaccuracies of the batch dynamic model. Figure 7 presents the Z component reference velocity and fit error to the January 19, 2010 reference orbit, and Fig. 8 shows the Z component reference velocity and fit error to the May 24, 2010 reference ephemeris. The velocity discontinuities are significant prior to the satellite failure, but do not exist in the post-failure data. This result indicates that the data discontinuities are because of regular maneuvers of the satellite and not to the method of data processing. It is confirmed that the Galaxy 15 reference ephemerides do not contain discontinuities after April 5, 2010.

It is of interest to note that Galaxy 15's motion out of the equatorial plane increased significantly after the spacecraft failed. Figure 9 compares the Z position before (January 1, 2010) and after (May 1, 2010) the spacecraft failure. The significant increase in out-of-plane motion is primarily because of the lunisolar gravitational perturbations that are not being corrected by ground control [25]. The effect of this perturbation on the orbit inclination can be investigated by approximating the inclination as the ratio of the maximum Z position to the corresponding

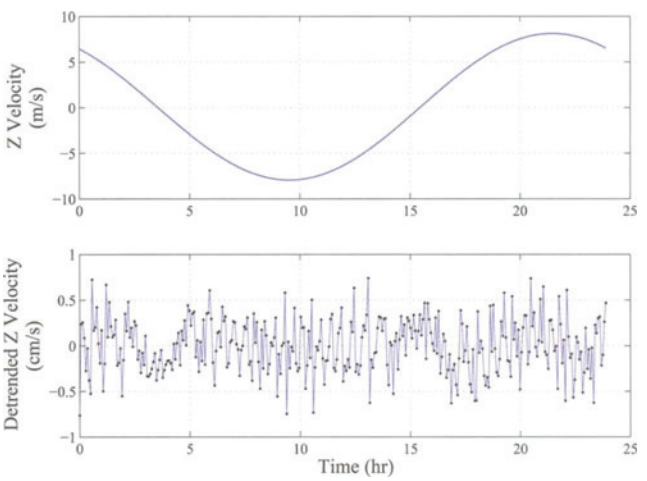

FIG. 8. Galaxy 15 Z Velocity and Fit Error (May 24, 2010).

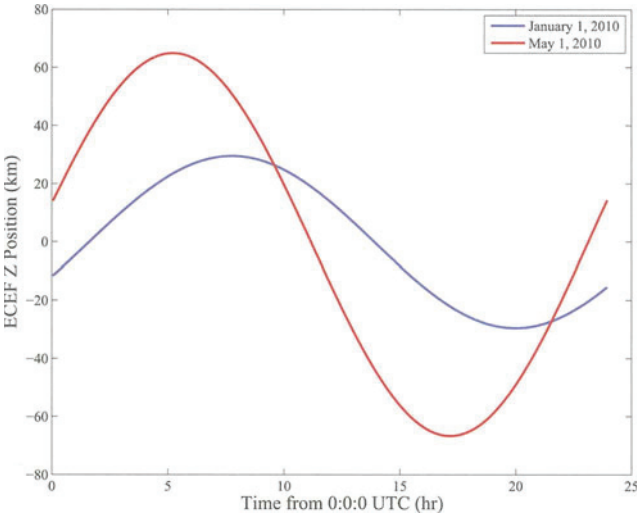

FIG. 9. Galaxy 15 Z Position Before and After Failure.

orbit radius. The orbit radius is computed as the norm of the ECEF position vector reported by the WAAS data files at the epoch of the maximum out-of-plane position. The pre-failure inclination is computed to be approximately 0.04 degrees, and the inclination increases to approximately 0.09 degrees by May 1. Recall that Galaxy 15 was controlled until April 5, 2010; the results show that by May 1 the orbit perturbations increased the inclination by a factor of about 2.25.

Achievable Angles-Only Orbit Estimation Accuracy

Observations of Anik F1R for May 2 through 3, 2010 are processed for all possible combinations of the tracking parameters. Two-day sliding windows of Galaxy 15 observations from May 2 through 30, 2010 are processed for all sampling intervals and nightly track length variations. Comparing the estimation solution accuracy for each tracking parameter combination allows for the empirical assessment of the impact of tracking duration, sampling frequency, and epoch location on estimation accuracy. Statistically assessing solutions over one month provides a metric of the solution distribution.

Anik F1R Analysis

Observations of Anik F1R spanning May 2 and 3, 2010 are processed to assess the estimator's performance while fitting over small, frequent maneuvers in the presence of mismodeled solar radiation pressure dynamics. The results are therefore an appropriate metric for determining the amount of tracking required for a given accuracy when observing an active geosynchronous communication satellite. The initial conditions for each epoch of May 2, 2010, produced by interpolating the reference ephemerides at the selected observation epoch, are shown in Table 4.

Figure 10 displays the 3D ECEF position error RMS values for Epoch 1 as a function of sampling time, where the curves represent different track lengths. In general, the position error increases as coverage arc length and sampling rate decrease. Track lengths of one to six hours produce very similar results. Ten-meter accuracy is achievable at short sampling intervals of 10 seconds and at least three

TABLE 4. Anik F1R Initial Conditions for Estimator Initialization (ECEF Frame)

Epoch (UTC on May 2, 2010)	X (km)	Y (km)	Z (km)	V_x (m/s)	V_y (m/s)	V_z (m/s)
00:01:04	−12526.484	−40255.336	−0.514	0.594	−0.693	−1.700
03:01:04	−12524.927	−40262.145	−16.777	−0.299	−0.494	−1.156
06:01:04	−12531.658	−40265.047	−23.142	−0.862	−0.037	0.036
09:01:04	−12541.629	−40263.335	−16.238	−0.912	0.319	1.175
12:01:04	−12550.042	−40258.757	−0.387	−0.594	0.503	1.609

hours of nightly track length. Tracking for only 10 minutes per night produces kilometer-level accuracy. Several tracking scenarios are able to achieve orbit accuracy on the order of 10 to 100 meters. For example, tracking continuously for 30 minutes at intervals of 10–30 seconds achieves 100-meter accuracy, and the same accuracy can be achieved by increasing the track length while decreasing the sampling interval. A long sampling interval of three hours is equivalent to tracking the object once at the beginning of the night and once again at the end, and 100-meter accuracy is possible even with this limited tracking scenario.

Figure 11 shows the 3D position error RMS values for the five observation epochs given a nightly track length of three hours. Tracking beginning at each epoch will cover a different portion of the entire orbit with no overlap. It is seen that the estimation accuracy is not significantly dependent on orbit epoch. This is expected as the unmodeled solar pressure, which is the primary source of error and directly affects the orbit eccentricity, does not significantly distort any sections of the orbit over the two-day period.

The Anik F1R analysis demonstrates that the batch estimator is capable of fitting over small maneuvers and can achieve excellent accuracy in the presence of realistically unmodeled dynamics. However, this analysis is a single case and provides no information regarding the solution error distribution.

Galaxy 15 Analysis

Next, one month of Galaxy 15 data is analyzed to avoid fitting over large station-keeping maneuvers while providing a set of two-day solutions. The mean position error and the error uncertainty is determined experimentally by statisti-

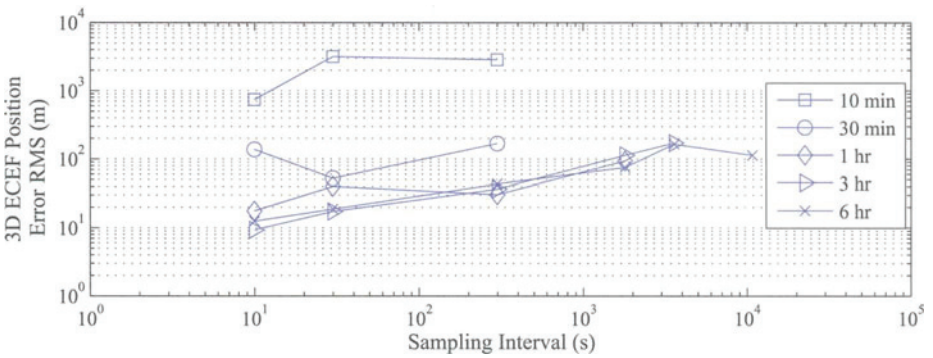

FIG. 10. Three-Dimensional ECEF Position Error RMS Value—Anik F1R.

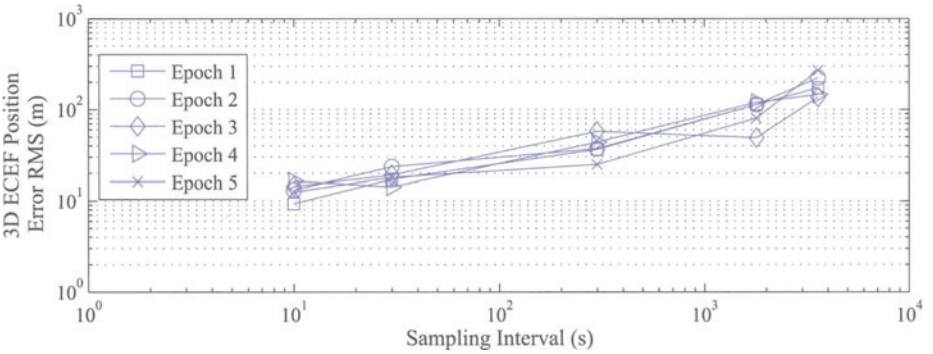

FIG. 11. Mean 3D ECEF Position Error RMS Value for Different Epochs—Anik F1R.

cally assessing the mean and standard deviation of a month of two-day fits. The May 2010 reference observations of Galaxy 15 are processed in sliding two-day windows such that the estimation statistics are determined from data sets covering May 1 and 2, May 2 and 3, etc. The data from May 7, May 16 and May 31 are discarded because the reference ephemerides are indicated to be of worse accuracy than desired. The accuracy must be at worst 10 meters for the data to be accepted for this analysis.

Figure 12 presents the mean 3D position error RMS values as a function of sampling interval and nightly track length. The 1σ uncertainty bounds for each track length are denoted by the dashed lines. The direct dependence of increased accuracy on shorter sampling interval and longer track length is strongly demonstrated in Fig. 12. The error uncertainty also decreases as the sampling interval decreases and track length increases. The uncertainty is on the order of the mean position error; for example, given a three-hour tract length and a sampling interval of 300 seconds, the mean error is approximately 100 meters with 1σ uncertainty bounds of approximately 20–200 meters.

The best possible accuracy is approximately 10 meters and is achievable given six hours of dedicated nightly tracking and a sampling interval of 10–30 seconds. The uncertainty for this case is on the order of a few meters. Tracking for only 10 minutes per night can produce solution accuracy on the order of several hundred meters given short sampling intervals, and this error can be reduced below 100 meters if the track length is increased to 30 minutes per night. It is shown that

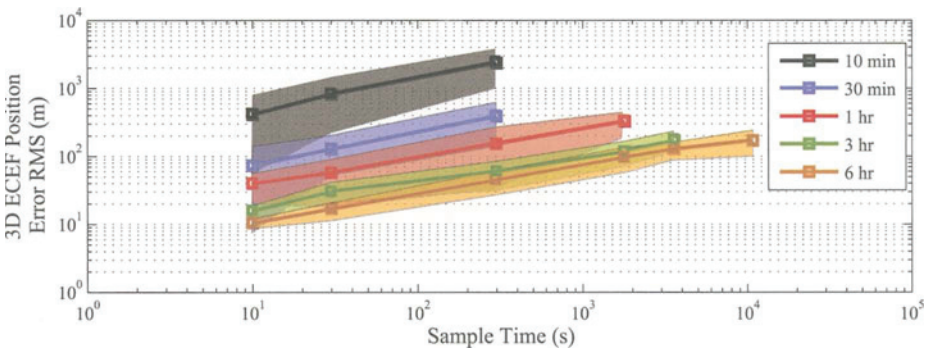

FIG. 12. Mean 3D ECEF Position Error RMS Value and 1σ Uncertainty Bounds—Galaxy 15.

several tracking scenarios can meet a given accuracy requirement between approximately 10 meters and 100 meters. Finally, tracking for longer than three hours per night does not provide a significant improvement in orbit accuracy, and 30 minutes to one hour of night tracking is sufficient to meet requirements for many geosynchronous operations [26].

Conclusions

This work has demonstrated using publicly-available accurate high-rate position and velocity point solutions for the characterization of geosynchronous orbit estimation accuracy given two days of ground-based optical observations. Novel case studies of two Wide Area Augmentation System satellites, Anik F1R and Galaxy 15, enabled a true test of accuracy using realistic vehicle motions for both controlled and drifting vehicles. As expected, longer tracking arcs and shorter observation intervals generally produced more accurate results; however, it was shown that arc lengths in excess of three hours and intervals shorter than 30 seconds have only marginal benefit. We estimate that 10-meter orbits can be readily generated using at least three hours of observations at intervals of at most 30 seconds for two nights, and 100-meter accuracy can be produced using at least 30 minutes of observations at intervals of 30 seconds.

These findings provide useful information for ground telescope operator planning, allowing for multiple geosynchronous objects to be tracked by a non-dedicated sensor over the course of the night without compromising accuracy. Short-term tracking is extremely useful when the sensor is unable to track the target object for longer than two days, such as when weather interrupts, or when an orbit solution is required in a short period of time. In the future we plan to extend the approach to the investigation of orbit estimation accuracy using space-based optical observations.

Acknowledgments

The authors would like to thank Dr. Grace Gao of Stanford University and Dr. Dennis Akos of the University of Colorado at Boulder for their contributions to parsing the WAAS messages. Thanks to Tim Schempp of Raytheon Company and Tom McHugh of the FAA Technical Center for providing valuable insight into WAAS operations and maneuvers. This work was funded by the National Defense Science and Engineering Graduate fellowship.

References

[1] JEHN, R., AGAPOV, V., and HERNANDEZ, C. "The Situtation in the Geostationary Ring," *Advances in Space Research*, Vol. 35, March 2005, pp. 1318–1327.

[2] SABOL, C. *A Role for Improved Angular Observations in Geosynchronous Orbit Determination*. Ph.D. Dissertation, University of Colorado, 1998.

[3] SABOL, C. and CULP, R. "Improved Angular Observations in Geosynchronous Orbit Determination," *Journal of Guidance, Control, and Dynamics*, Vol. 24, January-February 2001, pp. 123–130.

[4] SABOL, C., KELECY, T., and MURAI, M. "Geosynchronous Orbit Determination Using the High Accuracy Network Determination System (HANDS)," *Proceedings of the AAS/AIAA Space Flight Mechanics Meeting*, Wailea, Maui, Hawaii, February 2004.

[5] VISSER, B., SABOL, C., and DAHLKE, S. "Geosynchronous Orbit Determination Using High Accuracy Angular Observations," *Advances in the Astronautical Sciences*, Vol. 120, No. 1, 2005, pp. 527–541.

[6] MARSHALL, J.A., LEMONE, F.G., LUTHCKE, S.B., CHAN, J.C., COX, C.M., et al. "Precision Orbit Determination and Gravity Field Improvement Derived from TDRSS," *Proceedings of the AAS/AIAA Astrodynamics Specialists Conference and Exhibit*, Halifax, Nova Scotia, Canada, August 14–17 1995.

[7] VALLADO, D. and AGAPOV, V. "Orbit Determination Results from Optical Observations," *Proceedings of the 2010 International Conference for Astrodynamics Tools and Techniques*, May 2010.

[8] VALLADO, D., KELSO, T., AGAPOV, V., and MOLOTOV, I. "Orbit Determination Issues and Results to Incorporate Optical Measurements in Conjunction Operations," *Proceedings of the Fifth European Conference on Space Debris*, March 2009.

[9] AGAPOV, V., MOLOTOV, I., and TITENKO, V. "The ISON International Observations Network—Latest Scientific Achievement and the Future Works," *http://lfvn.astronomer.ru/report/0000037/001/index.htm*, February 2008.

[10] KAWASE, S. "Orbit Determination Accuracy for Optically Tracked Near-Synchronous Objects," *Proceedings of the International Symposium on Space Dynamics*, Biarritz, France, June 2000.

[11] TOMBASCO, J., AXELRAD, P., and JAH, M. "Specialized Coordinate Representation for Dynamic Modeling and Orbit Estimation of Geosynchronous Orbits," *Journal of Guidance, Control, and Dynamics*, Vol. 33, November 2010, pp. 1824–1836.

[12] MISRA, P. and ENGE, P. *Global Positioning System: Signals, Measurements, and Performance*, Chapter 2, Ganga-Jamuna Press, 2006.

[13] VAN DIERENDONCK, A.J. and ELROD, B. "Ranging Signal Control and Ephemeris Time Determination for Geostationary Satellite Navigation Payloads," *Proceedings of the ION National Technical Meeting*, 1994.

[14] CEVA, J. "Hughes Aircraft's Architectural Design of the Federal Aviation Administration Wide-Area Augmentation System: An International System," *Acta Astronautica*, Vol. 41, No. 4, 1997, pp. 335–345.

[15] VAN DIERENDONCK, A.J. and ENGE, P. *Global Positioning System: Theory and Applications*, Vol. 2, Chapter 4, American Institute of Aeronautics, Inc., 1996, pp. 117–142.

[16] Federal Aviation Administration, "Welcome to the William J. Hughes Technical Center WAAS Test Team," *http://www.nstb.tc.faa.gov/index.htm*, January 2010.

[17] Space News, "Orbital Blames Galaxy 15 Failure on Solar Storm," *http://www.spacenews.com/satellite telecom/*, April 2010.

[18] Space Now, "Zombiesat Has Three More Satellites in its Crosshairs," *http://www.spaceflightnow.com/news/n1007/25galaxy15/*, July 2010.

[19] C. News, "Zombie Satellite to do Another Flyby," *http://www.cbc.ca/technology/story/2010/11/04/zombie-satellite-flyby.html*, November 2010.

[20] Space.com, "'Zombie' Satellite Comes Back to Life," *http://www.space.com/9677*, December 29 2010.

[21] SOOP, E. *Handbook of Geostationary Orbits*, Chapter 2.3. Kluwer Academic, Dordrecht, 1994.

[22] Boeing, "Boeing: Satellite Development Center," *www.boeing.com/defense-space/space/bss/factsheets*, October 2010.

[23] Orbital, "Galaxy 12, 14 and 15 Fact Sheet," *http://www.orbital.com/NewsInfo/Publications/*, 2010.

[24] MONTENBRUCK, O. and GILL, E. *Satellite Orbits: Models, Methods, and Applications*, Chapter 3, p. 78. Springer, 2000.

[25] SOOP, E. *Handbook of Geostationary Orbits*, Chapter 4.2. Kluwer Academic, Dordrecht, 1994.

[26] POCHA, J. J. *An Introduction to Mission Design for Geostationary Satellites*, D. Reidel, Dordrecht, 1987.